Aerothermodynamic Design of High Speed Rockets

Samuel McAlees Jr.* and Randall C. Maydew†
Sandia National Laboratories, Albuquerque, New Mexico

The analytical methods, computer-code techniques, and experimental test procedures used in the aerothermodynamic design of high-speed rockets are presented. The thermal protection system designed for the Talos-Terrior-Recruit (TATER) rocket system is discussed. Comparisons between thermal response predictions and flight test experimental results for the TATER indicate that these methods can be used to design high performance rocket sytems.

Introduction

SEVERAL thousand single and multistage sounding rockets were launched in the past three decades for the study of endoatmospheric and exoatmospheric physics by U.S.A. universities and private companies, and by the NASA, Department of Defense (DOD), and Department of Energy (DOE), as well as by other countries. Sandia National Laboratories (SNL) initiated development of sounding and meteorological rocket systems in the late 1950's to support the high-altitude nuclear testing program.[1] In addition, rocket systems have been used extensively for aerodynamics research and development studies. Sixty rocket systems have been developed and 1400 rockets have been launched by SNL from 19 sites worldwide since 1957.

Aerodynamic heating analyses were conducted during the design of all high-performance (supersonic and hypersonic) rocket systems. Analytical methods and computer codes, developed for the aerothermodynamic design of nosetips and heat shields for high ballistic-coefficient reentry vehicles, were adapted for calculation of the aerodynamic heating of high performance rocket systems. Included are flowfield, aeroheating, chemistry, ablation, and heat conduction codes that predict vehicle pressure distributions, boundary-layer properties, heat-transfer rates, heat-shield ablation, and internal temperature responses. The analytical methods are used in the selection of thermal protection materials for vehicle nosetips, payload sections, flares, and fin leading edges. Results of theoretical analyses are supported by experimental test data obtained from radiant heat, arc-jet, wind tunnel, and flight tests. Data from these sources are used to characterize thermal protection materials and to verify theoretical predictions.

The analysis methods and experimental test procedures outlined above were applied in the design of the thermal protection system for the Talos-Terrior-Recruit (TATER)[2] rocket sytem. Of the rocket systems developed, the most severe aerodynamic heating problems encountered were in the design of the TATER system. The TATER, a three-stage, solid-propellant rocket, is capable of boosting a 32-kg payload to a velocity of 3200 m/s at an altitude of 4.3 km in 12 s. The system has onboard telemetry and a payload recovery system. Following a successful developmental flight test at the SNL Tonopah Test Range (TTR), Nev., in August 1973, an extensive operational TATER flight program was conducted during 1973-75 at Wallops Flight Center, Va., and at TTR. Twenty-six TATER flights were made through clear air and clouds to study reentry vehicle nosetip and heat shield materials.

This paper presents the method used to define the thermal protection system for the TATER, including comparisons between theoretical predictions and limited flight test data.

Design Methods

Several general application computer codes and experimental testing methods have evolved as design and analysis tools used to define thermal protection systems for high speed rockets, missiles, and reentry vehicles (RV). The methods used to design the TATER rocket system follow.

The NASA/AMES Flow Field (NAFF) code[3-5] is used to calculate the shock wave shape and distributions of pressure and other flow variables along the body and across the shock layer. The BLUNTY[6-9] code is used to compute vehicle cold-wall, heat-transfer rates. The Charring Material Ablation (CMA)[10-11] and Axisymmetric Transient Heat Conduction Material Ablation (ASTHMA)[12] codes are used to calculate the one- or two-dimensional, respectively, transient transport of thermal energy in a material that can ablate from the surface. The Aerotherm Chemical Equilibrium (ACE)[13] code uses JANAF[14] thermochemical data to calculate the chemical and thermodynamic state of a chemical system in equilibrium. The calculation flow chart is illustrated below (Fig. 1).

Experimental programs, conducted in ground-based test facilities, are used to further characterize candidate thermal protection system materials. Arc heater facilities[15-17] and a radiant heat facility[18] have been extensively used for material ablation tests of the nosetip materials [(ATJ-S), carbon phenolic, quartz phenolic, carbon-carbon] and heat shield materials (carbon phenolic, quartz phenolic, and silica phenolic) tested in the 26 TATER flights.

TATER Thermal Protection System Design

The most severe aerodynamic heating problems encountered in an SNL rocket development program have been in the design of the TATER[2] system (Fig. 2). The TATER is a solid-propellant, high-performance rocket vehicle designed to achieve maximum velocity at low altitude (~3.7 km; 12,000 ft) on an ascent trajectory. The vehicle derives its name from the Talos first-stage, Terrier second-stage, and Recruit third-stage motors. The first two stages are fin-stabilized; the third stage is flare-stabilized. The motor burn times for the first, second, and third stage are nominally 5.1, 4.2, and 1.6 s; the total impulses are 2633, 1103, and 253 kN-s, respectively. The TATER is 12 m long and weighs 3284 kg at launch. The cone-cylinder payload is 23.6 cm in diameter and 134.2 cm (nominal) in length. A complete analysis was conducted to

Submitted May 20, 1983; revision submitted June 7, 1984. This paper is declared a work of the U.S. Government and therefore is in the public domain.

*Supervisor, Aerothermodynamics Division.
†Manager, Aerodynamics Department.

determine the thermal protection required to provide satisfactory system performance over a range of intended uses in clear air and enhanced erosion environments. While the TATER environment does not match that encountered by an ICBM re-entry vehicle, it is severe enough to cause significant ablation, heat conduction, and thermal stress. Velocity history for the TATER is shown in Fig. 3. The preflight predicted velocities agree well with both the radar ground track and the onboard integrated-accelerometer velocity data. The heating environments encountered by the complete TATAR vehicle, (Fig. 4) including the nosetip, payload, and booster system; and the thermal response of these components to this environment, were determined. A stainless steel cap protects the Terrier's fin leading edge; the fin sidewalls are thermally protected with a 2.5-mm thickness of cast Dynatherm DE-350 (Sparesyl). The Recruit's motor and flare are protected with 2.2-mm and 11.4-mm coatings, respectively, of DE-350. Typical payload thermal protection (Fig. 5) consists of a graphite plug nosetip and 5.08-mm-thick graphite nose frustum, wrapped quartz phenolic (thickness decreases from 11.2 to 5.1 mm) along the conical heat shield and a 3.5-mm-thick DE-350 coating on the payload cylindrical section. The thermal protection system design of the nosetip, Recruit flare, and Terrier fins is discussed in detail since these components are subjected to the most severe pressure and heating conditions.

ATJ-S Graphite Nosetip Analysis

A developmental TATER vehicle was flown in clear air at the Tonopah Test Range to test both the overall system design and an instrumented ATJ-S graphite nosetip to obtain experimental recession and temperature data for comparison with analyses. The TATER was launched at an elevation angle of 15 deg; the maximum velocity of 3353 m/s (11,000 ft/s) occurred at 11 s at an altitude of 3523.5 m (11,560 ft). The payload was separated from the Recruit booster after apogee and a parachute system decelerated the payload to an impact velocity of 5 m/s (17 ft/s). A photograph of the recovered nosetip is shown in Fig. 6. The ATJ-S graphite plug was spring-loaded against a 9.0 deg cone half-angle ATJ-S graphite frustum. The nose plug has a spherical radius of 1.27 cm; the nose frustum was 0.508 cm thick. A 0.66-cm-thick carbon fiber-flake insulator protected the 0.102-cm-thick stainless steel substructure from the high temperatures of the ablator backface.

The test nosetip thermal instrumentation (Fig. 7) consisted of two ultra-miniature thermocouples and eight thermal sensors, manufactured by High-Temperature Instruments Division, Robinson-Halpern Corp., Plymouth Meeting, Pa. The thermocouple materials were tungsten/tungsten-26% rhenium. The wire elements, which were typically 0.002 cm in diameter, were insulated from each other by a quartz insulator. A tantalum sheath surrounded the assembly. The thermal sensors consisted of tungsten-5% rhenium/tungsten-26% rhenium thermocouples backed by carbon fiber-flake plugs, which were designed to duplicate the cross section of nosetip insulator. Good contact between the thermal sensors and the ablator backface was assured by slightly rounding the tip of the carbon fiber-flake plugs and by holding each sensor pair firmly in place with a circumferential spring. After the nosetip assembly was completed, the location of each temperature-measuring instrument and its contact with the ablator backface was verified by X-ray radiographs of the nosetip.

An acoustic gage, manufactured by K-West, Westminister, Calif., was used to measure the stagnation point recession during the flight. The device operates on the principle of a piezoelectric gage being shocked into mechanical oscillation at its natural frequency by a high-voltage pulse. The resulting shock pulse, a shear stress wave, is coupled into the stem of the nosetip (Figs. 5 and 7) where it propagates to the tip, is reflected, and returns to the piezoelectric gage. The elapsed time between the transmission of a pulse and its return is a measure of the length of the nosetip.

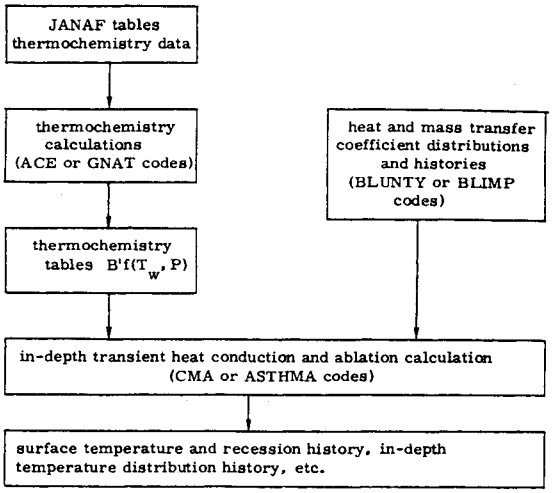

Fig. 1 Calculation flow chart.

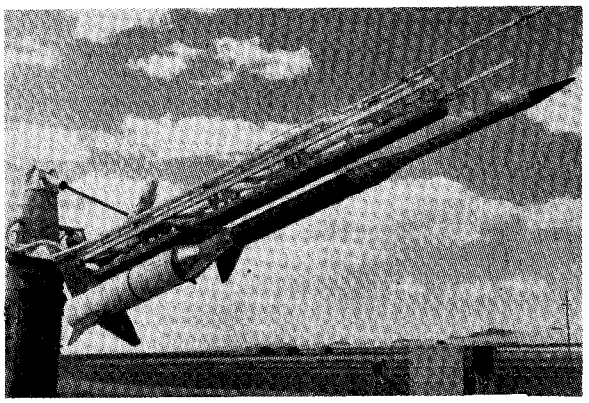

Fig. 2 TATER on launcher at Tonopah Test Range.

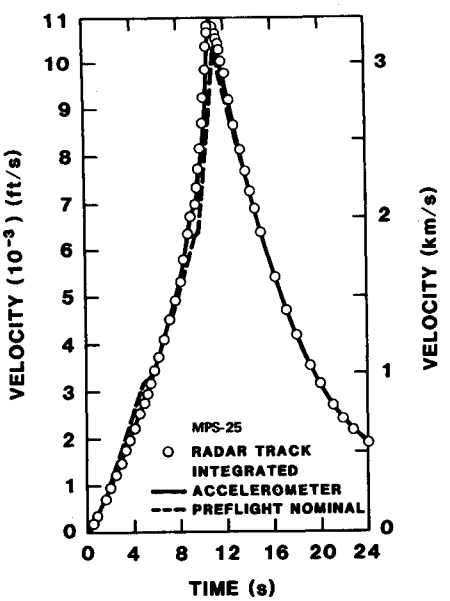

Fig. 3 TATER flight test velocity history.

Aerodynamic heating to the sphere-cone nosetip was calculated by the BLUNTY heating code for the TATER velocity history previously shown. Curve fits of the bow-shock shape and static pressure distributions obtained from the flow field program described by Lomax and Inouye[3] were used as input; therefore, entropy layer and pressure over-expansion effects

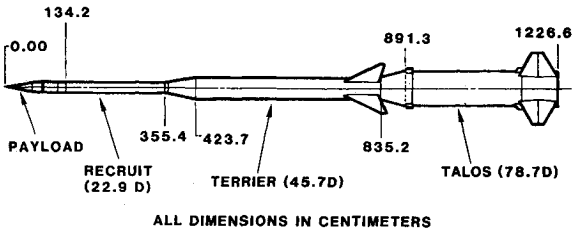

Fig. 4 TATER test vehicle.

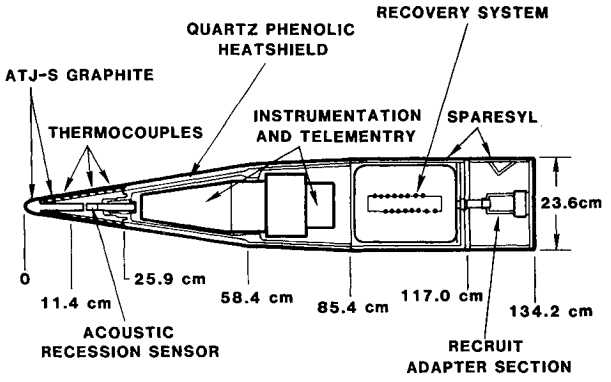

Fig. 5 TATER payload.

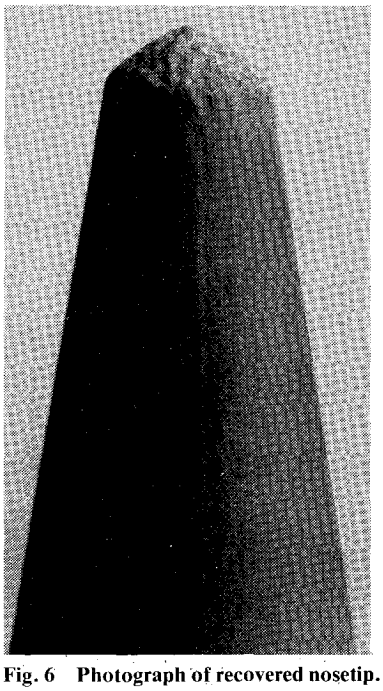

Fig. 6 Photograph of recovered nosetip.

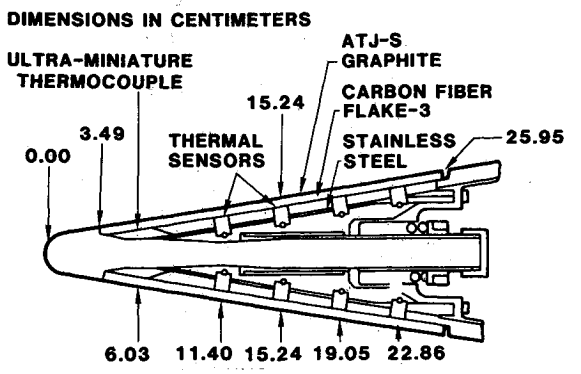

Fig. 7 TATER graphite nosetip experiment.

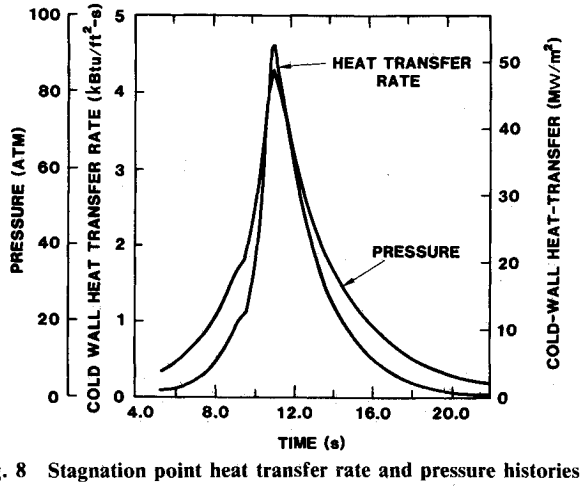

Fig. 8 Stagnation point heat transfer rate and pressure histories of TATER nosetip.

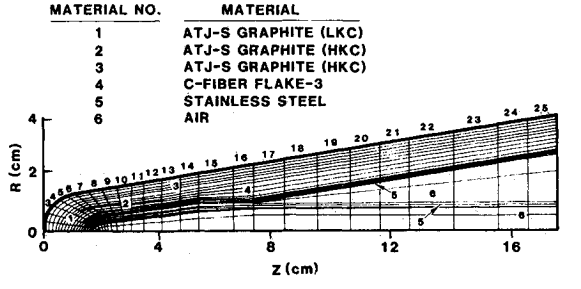

Fig. 9 Nosetip thermal model.

were included in the calculation. Aerodynamic heating and pressure histories were calculated for the stagnation point, 35 deg point, tangent point, and the 15.24-cm station. Stagnation point results are shown in Fig. 8. The ACE, CMA, and ASTHMA computer programs were used in the thermal analyses of the nosetip. The nosetip thermal model is shown in Fig. 9. LKC and HKC refer to the directionally dependent low and high thermal conductivity of ATJ-S graphite, respectively. Within the ASTHMA and CMA codes, the nonablating cold-wall heat-transfer coefficient is modified for the effects of blowing, wall temperature,[10] and surface roughness.[19] Adjustments in aerodynamic heating to account for departure from the sphere-cone configuration to the turbulent blunt biconic shape, which was predicted at 11 s into the flight, also were included.[20]

A plot of the x-y coordinates for the 0, 90, 180, and 270 deg roll angle profiles for the parachute-recovered nosetip are shown in Fig. 10. The symbols represent the average shape for the four profiles. A large portion of the nosetip profile can be represented by $y \sim x^{0.72}$ which is close to the $y \sim x^{0.75}$ relationship proposed by Welsh[21] for the stable-turbulent nose shape. The computed surface profile history of the nosetip for selected flight times and the average measured shape for the recovered nosetip are plotted in Fig. 11 for comparison with computed values. The computed recession at 22 s is in agreement with the measured recession of 1.44 cm of the recovered nosetip to within 0.1 mm. Figure 11 also shows the agreement between the computed and measured nosetip shapes. The measured stagnation point recession is compared with the one predicted (Fig. 12), illustrating fair agreement. The acoustic gage measurements[20] were corrected for longitudinal temperature gradients in the graphite plug since the wave speed is a function of temperature. Typical computed temperature profiles in the graphite plug are shown in Fig. 13.

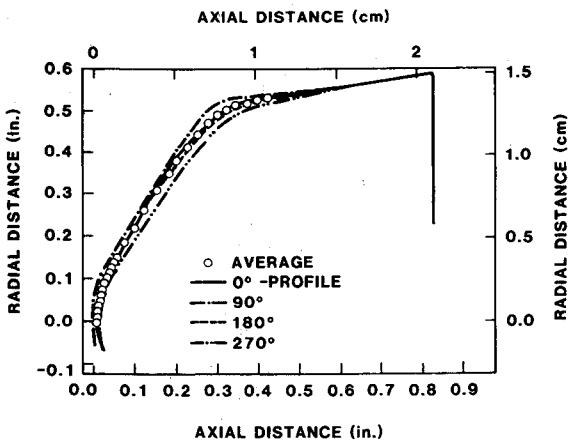

Fig. 10 Average shape determined from four roll angle profiles of recovered TATER graphite nosetip.

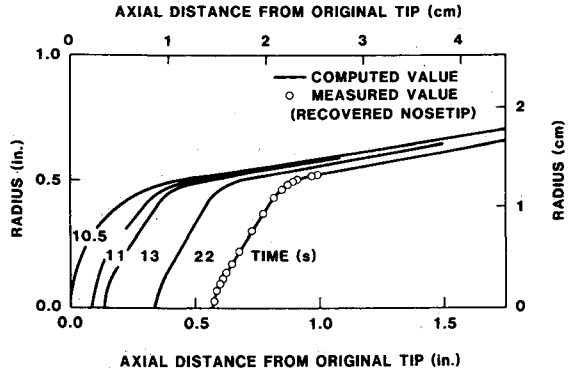

Fig. 11 Surface profile history of TATER graphite nosetip.

The scatter in the acoustic gage recession data was possibly due to acoustic impedance gradients caused by thermal gradients or wave cancellations caused by reflections from the changing nose shape.

Graphite plug temperature calculations[22] similar to Fig. 13 isotherms were made at several flight times to calculate the tensile thermal stress. The calculated maximum tensile stress was 24.5 MN/m^2 (3550 lb/in^2) at the 1.14-cm (0.45-in) station at 13 s. The minimum strength of the ATJ-S graphite at the temperatures at 13 s is approximately 27.6 MN/m^2 (4,000 lb/in^2). The intact recovered nosetip indicates that the calculated temperatures/thermal stresses were approximately correct.

The computed sidewall recession on the graphite frustum at two stations is shown in Fig. 14. The total sidewall recession, measured from the recovered nosetip (Fig. 6) compares well with the predicted values. Excellent graphite frustum backface [at 1.27 cm (0.5 in.) below the original surface] temperature data were recorded from seven thermocouples located at stations 11.4, 15.2, 19.1, and 22.9 cm (Fig. 7). Typical measured backface temperatures for stations 11.4 and 19.1 cm are compared with theoretical predictions in Figs. 15 and 16, respectively. Hochrein and Wright[20] concluded that boundary-layer transition occurred at the 6.0-cm nosetip station between 2.4 and 5 s, based on transition momentum Reynolds number correlations with NDAT, LORN, PANT, and STREET A transition criteria. The momentum thickness Reynolds number at 2.4 s at station 6.0 cm was about 500 compared with minimum required (transition criteria) of about 370. The unit freestream Reynolds number was 18.6×10^6 m. Backface temperatures were computed by assuming all laminar flow, all turbulent flow, with boundary layer transition at 5 s. Comparison of the backface temperature data (Figs. 15 and 16) with the computed values indicate the nosetip boundary-layer flow was turbulent over most of the flight. The comparison also indicates the thermal design is conservative since the predicted temperatures are higher than measured. This aerothermo design conservatism has been observed many times in designing thermal protection systems for rockets, missiles, and RVs. The mathematical models used do not properly account for all of the conductive, radiative, and convective heat paths or heat leaks; therefore, measured temperatures are usually less than computed temperatures.

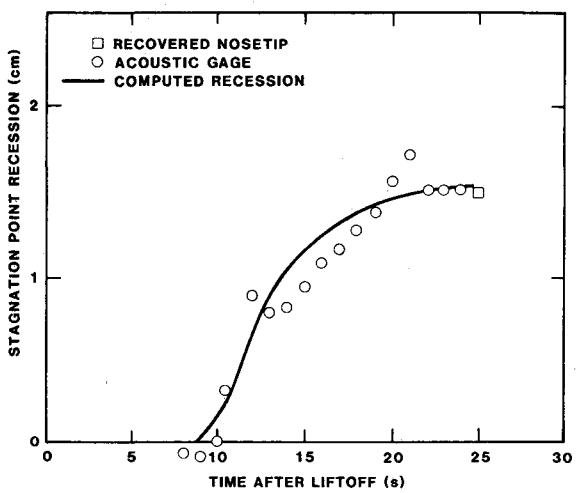

Fig. 12 Computed and measured stagnation point recession history.

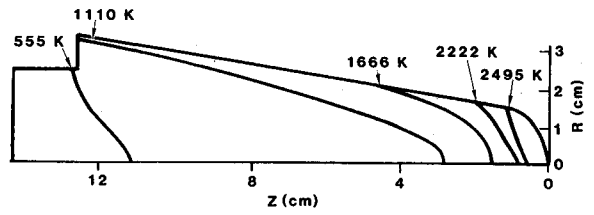

Fig. 13 Nosetip isotherms computed for 13 s of flight.

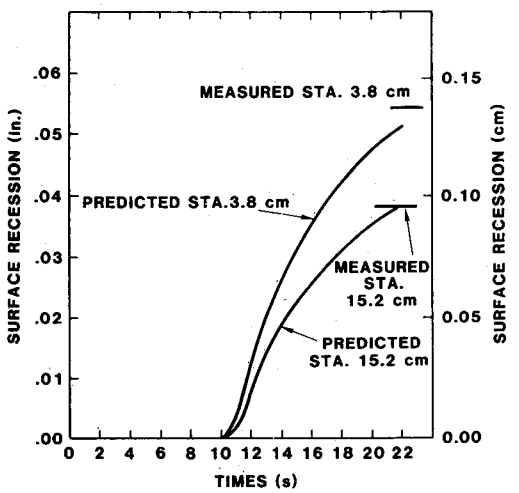

Fig. 14 Computed and measured sidewall recession history of TATER graphite nosetip.

Recruit Flare Analysis

The initial step in the flare analysis was the computation of pressure distributions over the payload sphere-cone, adapter

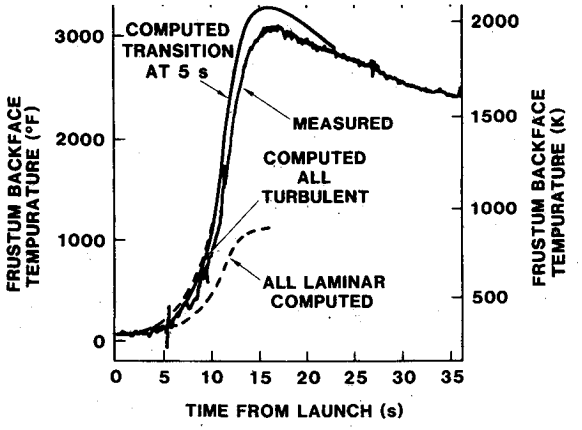

Fig. 15 Computed and measured backface temperature histories on nosetip at station 11.4 cm.

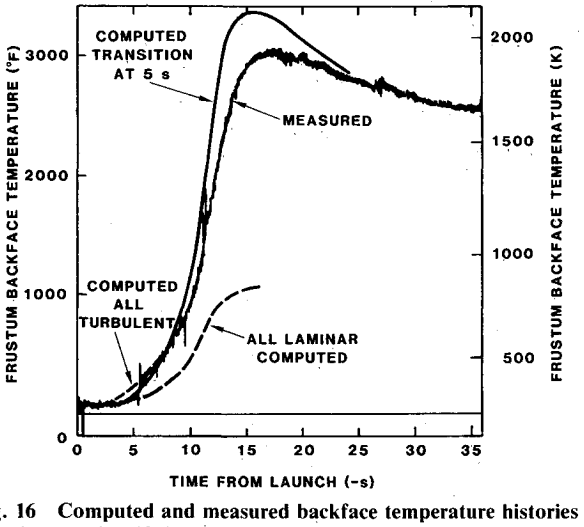

Fig. 16 Computed and measured backface temperature histories on nosetip at station 19.1 cm.

cone, and the Recruit cylinder-flare. Pressure distributions at Mach numbers of 3, 5, 6, 8, 10, and 12 were computed with the NAFF code. Pressure ratios as a function of nondimensional body length for selected Mach numbers are shown in Fig. 17. Cold-wall heat-transfer rates were predicted by using a sphere-cone-cylinder-flare version of the BLUNTY aerodynamic heating code and using the pressure distributions in Fig. 17 as inputs. For the higher Mach numbers, the maximum pressure and, therefore, the maximum heating occurs at approximately the midpoint of the 69-cm-long flare. Analysis of the nosetip frustum indicated that transition occurred on the frustrum early in the flight (at less than 5 s after launch). The freestream Reynolds number at the motor-flare juncture (based on a length of 356 cm) was approximately 56×10^8 at the maximum heating conditions, i.e., at $t = 11$ s. At this extremely high Reynolds number the turbulent boundary layer at the motor-flare junction would be thin, with little or no flow separation at the juncture. The analysis assumed no flow separation. The heat-transfer rates computed for the smooth wall were increased by a factor of 1.54 to include the effects of the increased heating[23] resulting from the 0.010-cm roughness of the Sparesyl. The calculated maximum heating rate 40.6 cm aft of the motor-flare juncture at 11 s is 11.9 MW/m^2. The heating rate of this station for the flight is illustrated in Fig. 18. The ablation material selected for the flare was Sparesyl DE-350, a room-temperature-cured, silicone-modified, epoxy-polyamide, low-temperature ablator. Formulated by a commercial firm,[24] it is suitable for

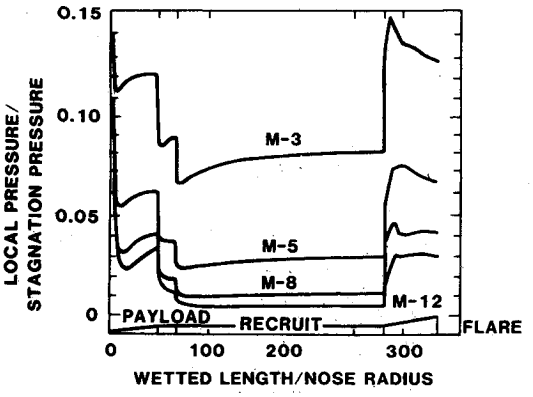

Fig. 17 Pressure distribution on recruit.

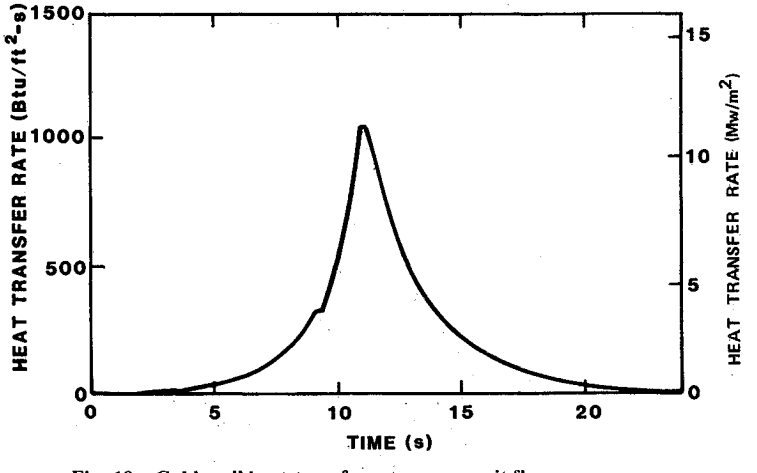

Fig. 18 Cold-wall heat-transfer rates on recruit flare.

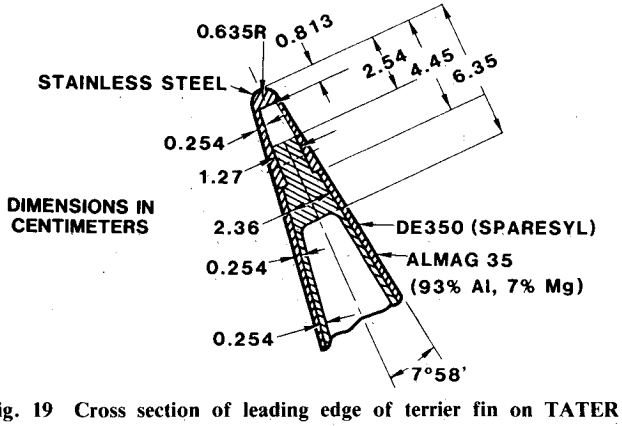

Fig. 19 Cross section of leading edge of terrier fin on TATER vehicle.

spraying or molding. Since the constituents of this material were not known in sufficient detail to allow a thermochemical ablation analysis, the heat-of-ablation (Q*) option of CMA[10,11] was used in the recession and temperature analyses. In a developmental flight test of the TATER test vehicle in August 1973, the Sparesyl ablator thickness on the 9 deg Recruit flare was 0.97 cm. A post-flight examination of the recovered flare revealed that all of the Sparesyl in a 15.2-cm-wide band had been removed from the flare midsection and that the almag substructure was exposed. This known removal of Sparesyl in a known flight environment, when used with the energy balance in CMA, allowed derivation of a thermochemical heat of ablation (Q*) of 2231 kJ/kg. The total Sparesyl recession obtained from a Recruit flare sub-

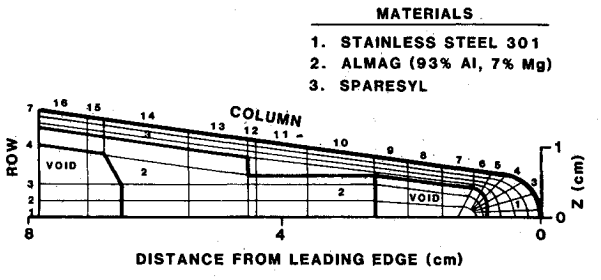

Fig. 20 Thermal model of terrier fin leading edge.

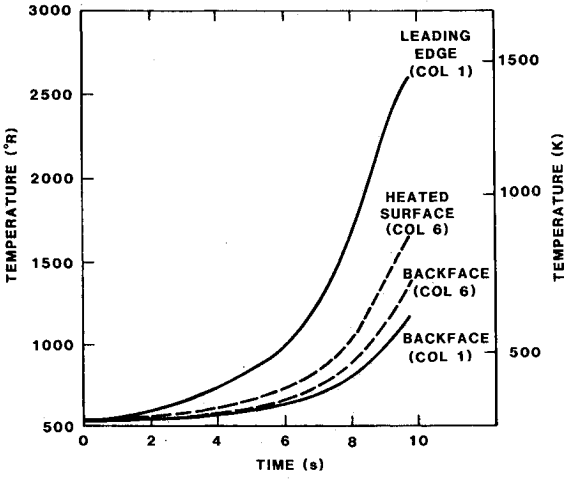

Fig. 21 Heated surface and backface steel temperatures on fin cap.

sequently flown at the Tonopah Test Range in clear air (and recovered) was 0.43 cm. This compares well with the computed value of 0.414 cm obtained for the same flight by the Q* approach above.

Terrier Fin Analysis

The Terrier fin (see Fig. 4) is a single-wedge chord with a 60 deg leading-edge sweep, a 30 deg trailing-edge sweep, and a clipped planform of 53.1-cm span. A drawing of the cross section of the Terrier's fin leading edge is presented in Fig. 19. The fin is an almag structure with a 0.25-cm-thick layer of Sparesyl ablator on the sides. The leading edge, which is swept 60 deg is thermally protected by a stainless steel cap. Cold-wall heat-transfer rates at the fin leading edge and around the swept cylindrical leading edge were computed according to the procedure presented in the "Aerodynamics Heat Transfer Handbook – Volume 1."[25] This procedure is based on the analysis of the heat transfer to a yawed cylinder by Beckwith and Gallagher.[26] In order to obtain the initial conditions for the heating analysis of the fin, the flowfield over the payload, Recruit, and Terrier was computed. The analysis indicated that the flow conditions at the fin were similar to those in the freestream; therefore, the heating rates were based upon the assumption that the Terrier fin was subjected to freestream flow. Turbulent flow was assumed at all times, and the heat transfer rates on the fin sides were computed by reducing the rate at the leading-edge tangent point according to the inverse fifth root of the surface distance, as suggested by turbulent flat-plate theory. The maximum cold-wall heat-transfer rates at the stagnation line and at the tangent point were 25 and 4.3 MW/m^2, respectively. The thermal model used for the two-dimensional heating analysis using the ASTHMA program is shown in Fig. 20. The spanwise heat transfer was neglected since the spanwise gradients are small compared to the chordwise variation in heat-transfer rate. The time-dependent local chordwise heat-transfer rates and the temperature-dependent materials properties for stainless steel, almag and Sparesyl were used with the thermal model in the analysis. The computed transient leading edge and typical surface temperatures with their respective backface temperatures of the stainless steel cap are shown in Fig. 21. The maximum computed temperature of the almag (column 10) was 400 K. The maximum computed mils of recession of the Sparesyl occurred in column 13; the almag is protected by a 100 mil cap of Sparesyl. The ablation of the Sparesyl was computed with CMA and the computed surface temperature and ablation were input as boundary conditions in ASTHMA. The maximum temperature computed for the stainless-steel (melting point 1683 K) leading edge of the Terrier fin was 1444 K; the maximum steel temperature estimated from a study of internal color distribution of a recovered fin leading edge was 1390 K. The recovered fin also indicated the almag is adequately protected by the steel cap and Sparesyl.

Conclusions

Results of the aerodynamic heating, thermal, and ablation analyses indicate the thermal protection system for all components of the TATER rocket are adequate. The computed stagnation point recession of the ATJ-S nosetip agrees well with the transient acoustic gage measurements and the measured recession from the recovered nosetip. The computed ATJ-S nosetip frustum surface recession at two stations agrees well with the measured values on the recovered nosetip frustum. Temperatures at the backface of the ATJ-S graphite nosetip frustum were measured at four longitudinal stations; the seven measured temperatures were slightly lower than the predicted temperatures. Transition occurred on the nosetip at a flight time of about 2.5 s, after which the entire TATER vehicle was immersed in turbulent boundary-layer flow. The measured ablation of Sparesyl from a recovered Recruit flare agreed well with the predicted values. The almag substructure of the Terrier booster fins was adequately protected thermally with a stainless steel nose cap and DE-350 (Sparesyl). The maximum computed temperature of the leading edge of the stainless steel Terrier fin was 1440 K compared with a measured (from a study of internal color distribution on the recovered fin) temperature of 1390 K. We conclude that the theoretical design methods presented herein can be utilized successfully to define thermal protection systems for high-speed rockets and missiles.

Acknowledgment

This work was supported by the U.S. Department of Energy. Appreciation is expressed to G.F. Wright, G.J. Hochrein, S.G. Beard, L.R. Rollstin, and M.L. Carnicom of Sandia National Laboratories.

References

[1] Fowler, G.A., Maydew, R.C., and Barton, W.R., "Sandia Laboratories Rocket Program—A Review, 1976," SAND76-0184, Sandia National Laboratories, Alburquerque, N. Mex., June 1976.

[2] Rollstin, L.R. and Fellerhoff, R.D., "Aeroballistic and Mechanical Design and Development of the Talos-Terrier-Recruit (TATER) Rocket System with Flight Test Results," SAND74-0440, Sandia Laboratories, Albuquerque, N.M. Feb. 1974.

[3] Lomax, H. and Inouye, M., "Numerical Analysis of Flow Properties About Blunt Bodies Moving at Supersonic Speeds in an Equilibrium Gas, 10964," NASA TR-R-204, July 1964.

[4] Inouye, M., Rakich, J.V., and Lomax, H., "A Description of Numerical Methods and Computer Programs for Two Dimensional and Axisymmetric Supersonic Flow Over Blunt-Nosed and Flared Bodies," NASA-TN-D-2970, 1965.

[5] Eaton, R.R. and Larson, D.E., "A Description of the Sandia Version of the NASA-Ames Flow Field Code: Input-Output and Storage Locations," SAND74—0097, Sandia Laboratories, Albuquerque, N.M. Dec. 1974.

[6] Hochrein, G.J., "A Procedure for Computing Aerodynamic Heating on Sphere Cones—Program BLUNTY, Volume II:

Equations, Operating Procedure, and Program Details," SC-DR-69-449, Sandia Laboratories, Albuquerque, N.M. 1969.

[7]Fay, J.A. and Riddell, F.R., "Theory of Stagnation Point Heat Transfer in Dissociated Air," *Journal of Aerospace Sciences,* Vol. 25, Feb. 1958, pp. 73-85.

[8]Kemp, N.H., Rose, P.H., and Detra, R.W., "Laminar Heat Transfer Around Blunt Bodies in Dissociated Air," Research Report 15, AVCO, Everett, Mass. 1958.

[9]Rose, P.H., Probstein, R.F., and Adams, M.C., "Turbulent Heat Transfer Through a Highly-Cooled Partially Dissociated Boundary Layer," Research Rept. 14, AVCO, Everett, Mass., 1958.

[10]Lauger, P.M., Kaestner, P.C., and Blackwell, B.F., "Operation Instructions for Charring Material Ablation Code," Sandia Laboratories, Albuquerque, N.M. 1973, SLA-73-0745.

[11]Moyer, C.B. and Rindal, R.A., "Finite Difference Solution for the In-Depth Response of Charring Materials Considering Surface Chemical and Energy Balances," Final Report No. 66-7, Part II, Aerotherm Corporation, Mt. View, Calif. 1967.

[12]Moyer, C.B., Blackwell, B.F., and Kaestner, P.C., "A User's Manual for the Two-Dimensional Axisymmetric Transient Heat Conduction Material Ablation Computer Program (ASTHMA), SC-DR-70-510, Sandia Laboratories, Albuquerque, N.M., 1970.

[13]Powers, C.A. and Kendall, R.M., "User's Manual Aerotherm Chemical Equilibrium (ACE) Computer Program," Aerotherm Corporation, Mt. View, Calif. 1969.

[14]Data Sheets published periodically by JANAF Thermochemical Panel, DOW Chemical USA, Thermal Research, Midland, Mich.

[15]Sheldahl, R.E. and Wright, G.F. Jr., "A Channel Test Device for Arc Jet Material Ablation Studies," *Journal of Spacecraft and Rockets,* Vol. 8, Nov. 1971.

[16]Painter, J.H., and Ehmen, R.J., "Development of a High Performance Arc Heater for Ground Testing Advanced Strategic Reentry Vehicle Components," MDRL 71-1, McDonnell Douglas Research Laboratories, St. Louis, Mo., 1971.

[17]AVCO Hyperthermal Simulation Capabilities," AVSC 047-70-CA, AVCO Systems Division, Everett, Mass.

[18]Adams, P.E. et al., "Sandia Laboratories Radiant Heat Facility," SAND79-2181, Sandia National Laboratories, Albuquerque, N.M., 1980.

[19]Powers, C.A., "Analysis of PANT Series A. Rough Wall Calorimeter Data, Part I," Aerotherm Report 73-80, Aerotherm Corporation, Mt. View, Calif., 1973.

[20]Hochrein, G.J. and Wright G.F., Jr., "Postflight Analysis of the TATER Nosetip Boundary-Layer Transition and Ablation Experiment," SAND75-0207, Sandia Laboratories, Albuquerque, N.M., 1975.

[21]Welsh, W.E., "Shape and Surface Roughness Effects on Turbulent Nosetip Ablation," *AIAA Journal,* Vol. 8 Nov. 1970.

[22]Beard, S.G., Carnicom, M.L., McAlees, S., Randall, D.E., and Hochrein, G.J., "Thermal Analyses of the TATER (Talos-Terrier-Recruit) Test Vehicle Graphite Nosetip, Flare and Fins," SAND74-0176, Sandia Laboratories, Albuquerque, N.M., Nov. 1974.

[23]Powers, C.A., "Surface Roughness Effects on Reentry Heating," TM-71-10, Aerotherm Corp., Mt. View, Calif. July 1971.

[24]"Dyna-therm DE-350 Ablative Coating," Preliminary Data Sheet, Flamemaster Corporation, Sun Valley, Calif. August 1977.

[25]"Aerodynamic Heat Transfer Handbook—Volume I," Document No. D2-9514, Boeing Airplane Company, Seattle, Wash., 1961.

[26]Beckwith, I.E. and Gallagher, J.J., "Local Heat Transfer and Recovery Temperatures on a Yawed Cylinder at a Mach Number of 4.15 and High Reynolds Numbers," NASA TR-R-104, 1958.

AIAA Meetings of Interest to Journal Readers*

Date	Meeting (Issue of *AIAA Bulletin* in which program will appear)	Location	Call for Papers†
1985			
June 19-21	**AIAA 20th Thermophysics Conference** (Apr)	Fort Magruder Inn Williamsburg, VA	Sept 84
July 8-10	**AIAA/SAE/ASME 21st Joint Propulsion Conference** (May)	Doubletree Inn Monterey, CA	Aug 84
July 15-17	**AIAA 7th Computational Fluid Dynamics Conference** (May)	Westin Hotel Cincinnati, OH	Oct 84
Aug 12-14‡	**AAS/AIAA Astrodynamics Conference**	The Lodge Vail, CO	Nov 84
Aug 19-21	**AIAA Atmospheric Flight Mechanics Conference** (June)	Snowmass, CO	Nov 84
Sept 2-6‡	**27th International Symposium on Air Breathing Engines (ISABE)**	Beijing, China	
Sept 30- Oct 2	**AIAA/DGLR/JSASS 18th International Electric Propulsion Conference** (July)	Ramada Hotel Alexandria, VA	Dec 84
Oct 7-12	**36th International Astronautical Congress (IAF)**	Stockholm, Sweden	Jan 85
Oct 8-10	**AIAA/NASA Earth Observing Systems (EOS) A Potential User of Space Station** (July)	Pavilion Tower Virginia Beach, VA	Dec 84
Oct 14-16	**AIAA Applied Aerodynamics Conference** (Aug)	Clarion Hotel Colorado Springs, CO	Jan 85
Nov 13-15	**AIAA Shuttle Environment and Operations II Conference** (Aug)	Houston, TX	Feb 85

*For a complete listing of AIAA meetings, see the current issue of the *AIAA Bulletin.*
†Issue of *AIAA Bulletin* in which Call for Papers appeared.
‡Co-sponsored by AIAA. For program information, write to: AIAA Meetings Department, 1633 Broadway, New York, N.Y. 10019.